

Photonic reservoir computing based on micro-ring resonators for direction finding of unmanned aerial vehicles

Jingda Yang (杨京达)^{1,2,†}, Zike Chen (陈子可)^{1,2,†}, Jiqiang Mao (毛继强)^{1,2}, Shufei Han (韩书菲)^{1,2}, Qianzhu Xia (夏寒翥)³, Weihong Shen (沈微宏)^{1,2*}, Min Gu (顾敏)^{1,2**}, and Qiming Zhang (张启明)^{1,2***}

¹School of Artificial Intelligence Science and Technology, University of Shanghai for Science and Technology, Shanghai 200093, China

²Institute of Photonic Chips, University of Shanghai for Science and Technology, Shanghai 200093, China

³School of Mechanical Engineering, University of Shanghai for Science and Technology, Shanghai 200093, China

[†]These authors contributed equally to this work.

*Corresponding author: shenweihong@usst.edu.cn

**Corresponding author: mingu@usst.edu.cn

***Corresponding author: qimingzhang@usst.edu.cn

Received June 11, 2025 | Accepted August 1, 2025 | Posted Online November 7, 2025

Unmanned aerial vehicles (UAVs) face challenges in real-time high-precision tasks such as data acquisition and environmental monitoring, which demand low-latency decision-making and high-speed data transmission. A photonic reservoir computing (PRC) system based on silicon-integrated micro-ring resonators (MRRs) was demonstrated for UAV flight direction recognition, achieving an accuracy of 95.6%. The proposed PRC exhibits short-term memory effects, enabling the detection of subtle changes in flight direction. The PRC operates at the MHz-rate with milliwatt-level power consumption, enabling photonic edge computing with high speed and energy efficiency, providing UAVs the potential to make decisions autonomously and avoid external interference when operating in extreme environments.

Keywords: unmanned aerial vehicle; optical computing; micro-ring resonator; reservoir computing.

DOI: [10.3788/COL202523.121301](https://doi.org/10.3788/COL202523.121301)

1. Introduction

Unmanned aerial vehicles (UAVs)^[1] are commonly used to perform real-time, high-precision data acquisition, processing, and analysis tasks, such as map generation, environmental monitoring, and target recognition. These tasks require high computational power and low latency, especially when UAVs operate in harsh environments. As shown in Fig. 1(a), the raw data of videos collected by UAVs needs to be transmitted to ground controllers and base stations for data processing. After that, the decisions and control signals are sent back to the UAVs to direct their movements. Limited by transmission distance and communication bandwidth, the back-and-forth communications and data processing experience a delay of hundreds of milliseconds, and are also vulnerable to external signal interference or eavesdropping.

Edge computing^[2] addresses this issue by pushing computing tasks closer to the data source, allowing UAVs to perform data preprocessing and analysis locally, significantly reducing data transmission latency and alleviating reliance on remote

computing resources. However, edge computing devices are still limited by the processing power of traditional hardware, particularly when facing complex image processing, deep learning inference, and high-resolution video analysis. Existing electronic computing hardware often fails to meet the demands for efficiency and low latency in such tasks.

Over the past decade, optical computing^[3,4] has shown significant advantages in various fields due to its high parallel computing capacity and extremely low latency. Compared to traditional electronic computing, optical computing enables faster parallel computation, particularly for large-scale data streams and high-dimensional computing tasks, making it well-suited for image, video, and sensor data processing. As shown in Fig. 1(b), by employing the optical edge computing engine, UAVs can perform computational tasks locally instead of sending the data back and waiting for controlling signals, thereby reducing the latency and enhancing the capabilities of autonomous decision making and execution efficiency. Additionally, CMOS-compatible silicon photonic integrated

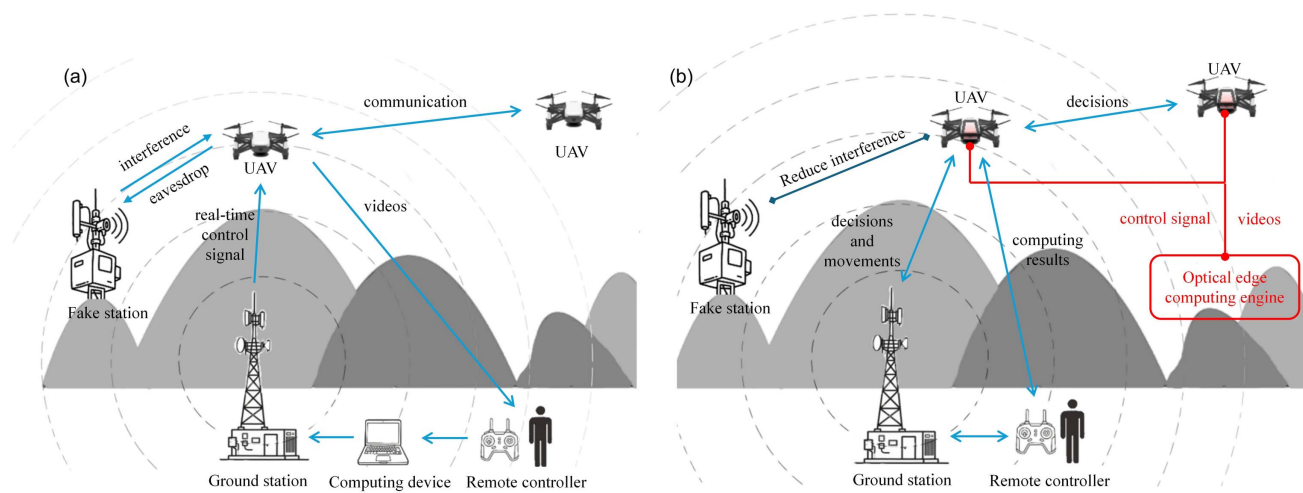


Fig. 1. (a) Traditional controlling model of UAVs, relying on the back-and-forth communication and the ground controller for data processing. (b) Schematic of a UAV equipped with an optical edge computing engine, which processes signals locally, enabling low latency and strong anti-interference communication.

chips offer strong support for hardware implementation in optical edge computing. Currently, the computing power of optical computing has exceeded 10 TOPS (tera operations per second)^[5]. It can be estimated that UAVs equipped with optical edge computing engines can process data within the order of 10 μ s, which is more than three orders of magnitude faster than the latency of traditional communication.

Reservoir computing (RC)^[6,7] is a variant of recurrent neural networks (RNNs) that addresses issues such as gradient explosion and vanishing gradients during training. A reservoir computing system consists of three main components: the input layer, the reservoir, and the readout layer, as shown in Fig. 2. The input layer encodes external data and passes it to the reservoir, where the fixed weights map the data to a high-dimensional feature space. The output states from the reservoir are then passed to the readout layer, and only the weights of the output layer need to be trained to perform the target task, making it particularly suitable for hardware implementation in edge computing scenarios.

In this paper, a photonic reservoir computing (PRC) system based on silicon-integrated micro-ring resonators (MRRs) was demonstrated for discriminating UAV flight directions. The optical input-output plane of the MRR exhibits delayed nonlinear phenomena, providing the natural nonlinearity and short-term memory effects, which help to avoid feedback loops when constructing a photonic reservoir and establish connectivity between optical virtual nodes. On this basis, the PRC was applied to classify UAV flight directions, achieving an experimental classification accuracy of 95.6%, outperforming traditional classification models such as ridge regression. Additionally, due to its unique short-term memory effect, the model captures slight variations in UAV flight direction, resulting in reduced Euclidean distances, indicating that the prediction error is smaller compared to conventional models. This work suggests that the MRRs-based PRC provides the potential for UAVs to perform tasks and make decisions on the edge side without relying

on remote control, enhancing their abilities in autonomous decision-making and anti-interference resilience especially when operating in extreme or specialized environments.

2. Theoretical Simulations

The PRC system is composed of three main parts: the input layer, the photonic reservoir, and the readout layer. To apply the proposed PRC for UAV direction recognition, we manually collected flight videos of a UAV flying in different directions. We selected two commercial UAV products and controlled their flight direction and speed using Python code. One UAV was used to capture another UAV's flight in four directions: upward, downward, leftward, and rightward. A total of 200 videos (1280 \times 720 resolution) were recorded. Three frames extracted from the flight sequences were selected as a data sample. Through a series of preprocessing methods, including removing invalid videos, image segmentation, image smoothing, feature extraction, and down-sampling, a dataset consisting of 160 valid samples, where each frame had the size of 48 pixel \times 27 pixel, was obtained. The processed 160 data samples were divided into four groups based on the flight directions and input into the photonic reservoir for simulation.

The next step is to use the nonlinear dynamic response of the MRR to construct the photonic reservoir. A theoretical model of the silicon-integrated MRR based on the coupled-mode theory (CMT)^[8] was investigated in order to construct the PRC system. The CMT equations considering two-photon absorption, free carrier absorption, free carrier dispersion, and thermo-optic effect^[9–11] were employed to analyze the nonlinear dynamics of the MRR. The Kerr effect is neglected here since it has a minimal impact on the refractive index. In the simulation, we used a thermal relaxation time of 550 ns^[12] and a free carrier lifetime of 6.5 ns^[13]. By solving the eigenvalue matrix, the boundary conditions of optical bistability (BI) and self-pulsing (SP)^[13] were

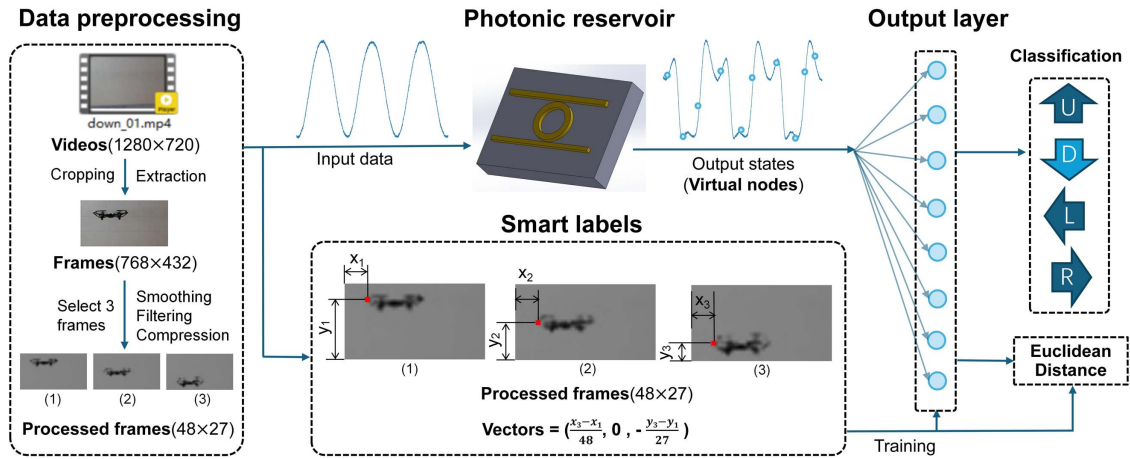


Fig. 2. Schematic flowchart of the MRR-based PRC system for UAV direction finding. Flight videos of a UAV flying in four directions were captured, and frames were extracted, preprocessed, and down-sampled. The samples were grouped by direction, input into the photonic reservoir, and processed with ridge regression. “Smart labels” based on motion vectors improved labeling accuracy and classification performance.

obtained, so as to choose an appropriate range of incident optical power, avoiding the appearance of SP in the photonic reservoir. The nonlinear response of MRR is discussed in the subsequent experimental results.

The training data is loaded onto the intensity-modulated optical input signals with average power P_{in} . After transmitting through the bus waveguide of the MRR, the time sequences of optical output signals carry the state of the photonic reservoir and eventually pass through the readout layer for classification. The output signals from the photonic reservoir are down-sampled into virtual nodes, which are then fed to the readout layer for training. Ridge regression^[14] is used during the training process instead of linear regression to prevent overfitting and improve numerical stability. Considering the instability of UAV flight directions, we improved the labeling method by replacing the human-labeled flight directions with “smart labels” based on the motion vectors. The relative motion vectors were calculated by the displacement of specific pixels in relation to the total frame. By means of the “smart labels”, the accuracy of the flight direction labels was enhanced, resulting in an improved classification performance eventually.

The dataset was split into 60% for training and 40% for testing. The Euclidean distance^[15] between the predicted and actual vectors of UAV flight directions was employed to quantitatively analyze the training results of the smart labels. For example, when a UAV ascends, small shifts to the left or right occur due to the aircraft’s body instability. While the classification of motion direction can only distinguish large movements, a smaller Euclidean distance indicates a stronger ability to capture subtle offsets, even with high classification accuracy. To demonstrate the role of the MRR’s hysteresis response in the PRC, we calculated the PRC results with the MRR operating in the hysteresis response region or the high-frequency linear region. When the MRR operates in the linear region, the RC behaves as a linear system, where the input data is directly trained using ridge regression. The classification results based on the

simulation model are shown in Fig. 3(a) and 3(b). The proposed photonic reservoir system based on MRR achieves an average accuracy of 97.5% for the four flight directions, outperforming the results achieved by the system without PRC only with a ridge regression model through a linear system. Additionally, as shown in Fig. 3(c), compared to the high-frequency linear case, the hysteresis of MRR improves the accuracy of the classification results and reduces the Euclidean distance between the predicted and actual values of the motion direction. This indicates that the MRR-based photonic reservoir possesses a short-term memory effect, allowing the model to recognize small changes in UAV flight direction.

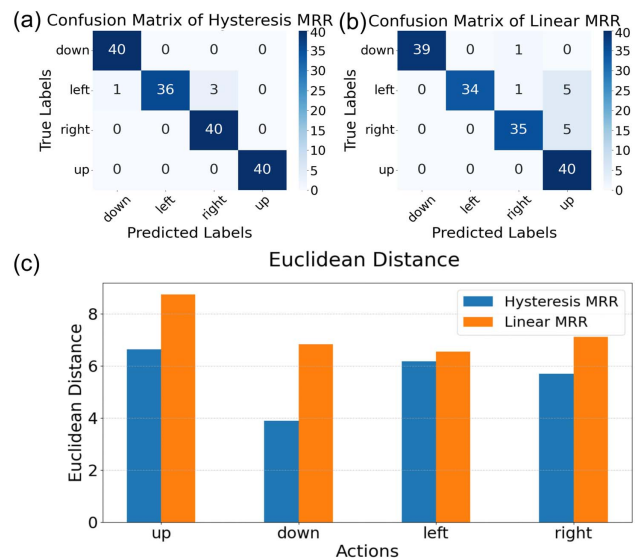


Fig. 3. Accuracy of the simulation with hysteresis (a) and linear MRR (b) in the photonic reservoir, and (c) comparison of the Euclidean distance between the predicted and actual direction vector values.

3. Experimental Validation

The simulation results demonstrate the nonlinear and memory characteristics of the MRR-based photonic reservoir, as well as the effectiveness of the self-collected dataset. On this basis, we conducted an experimental validation. The MRRs were performed on a 220-nm-thick silicon-on-insulator (SOI) photonic integrated chip, fabricated by the Advanced Electronic Materials and Devices Center (AEMD)^[16]. For measurement of the photonic hysteresis behavior, an MRR with a radius of 20 μm , a gap of 200 nm in the coupling region, and a quality factor of 1.1×10^4 was selected. The experimental setup is shown in Fig. 4. A continuous-wave (CW) tunable laser source (TLS) working at C-band was used. The input data was modulated onto the optical intensity using a Mach-Zehnder modulator (MZM), then amplified by a fixed-gain erbium-doped fiber amplifier (EDFA). Then, the optical power input to the on-chip photonic reservoir was adjusted using a variable optical attenuator (VOA) before that. The amplified optical signals passed through a 1×3 optical power splitter, with 15% of the power sent to an optical power meter (OPM) for monitoring the input power, and another 15% used for photodetector 1 (PD1) to detect the input optical signal through an oscilloscope (OSC) as a reference. The remaining 70% of the power was coupled through a grating coupler into the bus waveguide of the MRR on the silicon photonic chip, with approximately 4-dB loss in the coupling process. Finally, the optical signal directly going through the bus waveguide of the MRR was coupled out through another grating coupler, detected by photodetector 2 (PD2), and the waveform was monitored in the real-time oscilloscope.

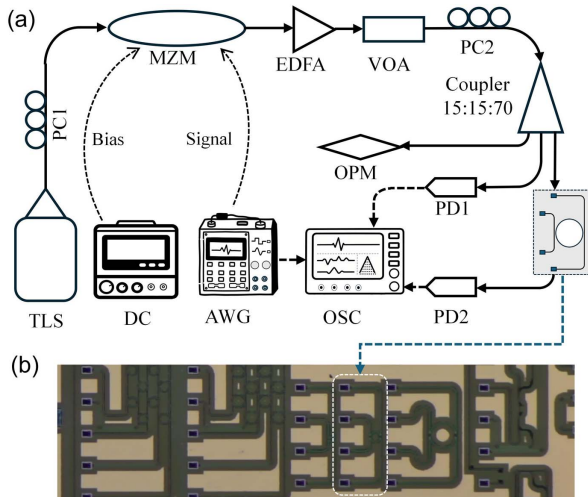


Fig. 4. (a) Schematic of the experimental setup used for measuring the hysteresis loop at different frequencies, including the following equipment: TLS [tunable laser source], MZM [Mach-Zehnder modulator], PC [polarization controller], EDFA [erbium-doped fiber amplifier], VOA [variable optical attenuator], PD [photodetector], OPM [optical power meter], AWG [arbitrary waveform generator], and OSC [oscilloscope]. (b) Microscope of the fabricated MRRs for the experiment.

The experimental measurement of the optical input-output plane is illustrated in Figs. 5(a) and 5(b), where the input light was a sinusoidal intensity-modulated signal with 1-MHz modulation frequency. We can see that the output response of MRR shows a clear bistability, that is to say, the output switches between two stable states and exhibits significant nonlinear responses and memory effects. Throughout the process, the system demonstrates nonlinear characteristics and short-term memory effects, providing potential support for photonic neuromorphic computing, particularly in the application of temporal signal processing^[17,18]. The unique nonlinear properties and short-term memory effects observed in the MRR provide a strong foundation for the development of PRC systems.

Based on this, we employed the self-collected UAV dataset shown in Fig. 2 for the classification task of UAV flight directions. The experimental setup followed a similar method to that in Fig. 4. Each dataset consists of three videos, each with three frames of 48 pixel \times 27 pixel, which are normalized and flattened into a 1D vector. To identify the start positions of the data during experiments, a header was added at the beginning of each dataset, with a relatively low amplitude to avoid interfering with the afterward signal response. The input data was loaded into the arbitrary waveform generator (AWG) at a sampling rate of 1 MSa/s and converted into optical time-domain signals using the MZM. The modulation range of optical input power was adjusted according to the power range of the hysteresis loop we obtained in Fig. 5(a), so as to maximize the utilization of

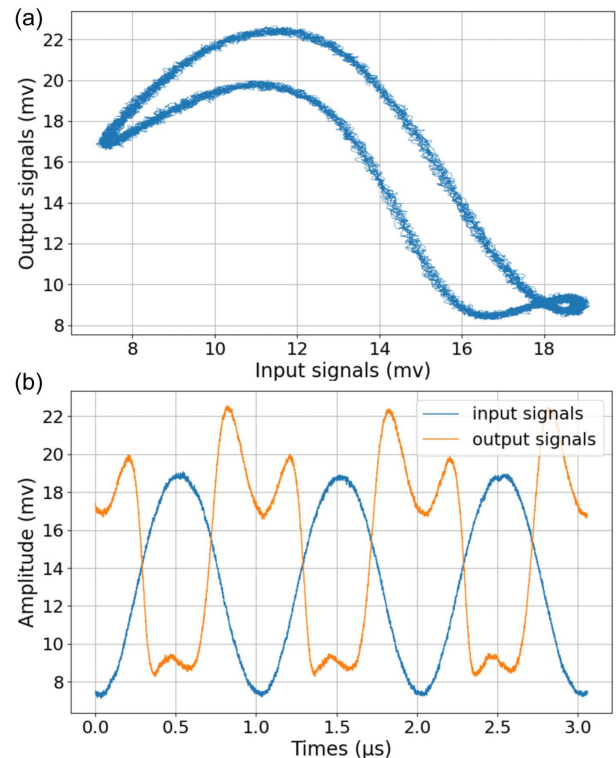


Fig. 5. (a) Hysteresis loop of the optical input and output signals. (b) Temporal sequences of the optical input and output signals, which are displayed as the electrical signals collected by the oscilloscope.

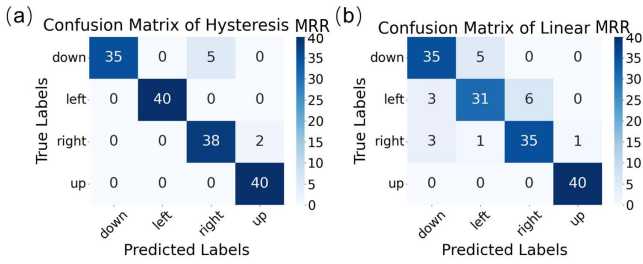


Fig. 6. Comparison of the classification accuracy of ridge regression for flight direction with hysteresis (a) and linear (b) MRR photonic reservoirs using the post-experimental optical signal.

the nonlinearity and memory of the MRR. During the experiment, the average input power of the MRR was 12.5 dBm. We used PDs and an OSC to capture the output signals from the MRR, which reflected the dynamic states of the photonic reservoir.

To preserve the integrity and complexity of the photonic reservoir’s temporal states, the optical output sequence was sampled at equal intervals into n virtual nodes (the number of nodes matching the input data), which were then input to the readout layer. This method comprehensively captures the dynamic responses of the reservoir to the entire sequences, thereby enhancing the processing and recognition capabilities

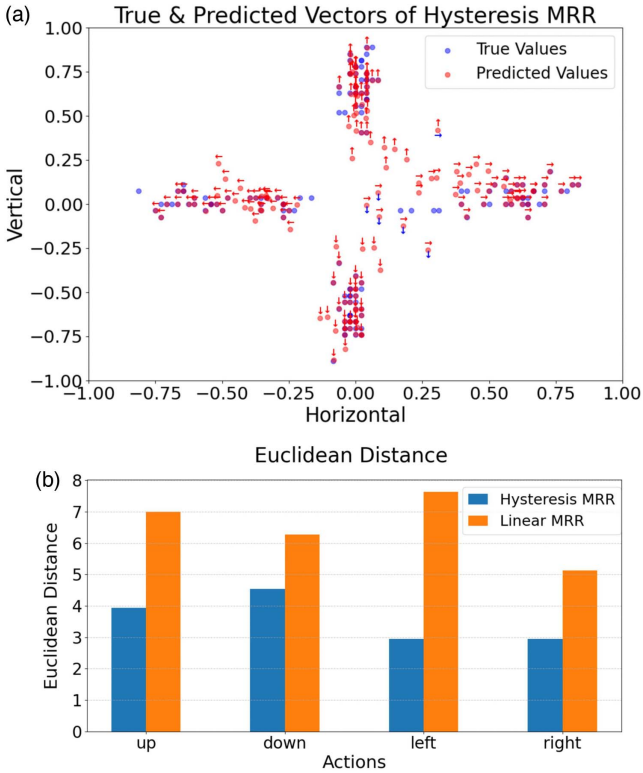


Fig. 7. (a) Comparison of the predicted and actual values for the four flight directions after passing through the MRR, with blue points representing the true values of the misclassified objects. (b) Comparison of the Euclidean distance between the predicted and actual flight direction vectors, using hysteresis and linear MRRs.

of the PRC system. The output signals of the photonic reservoir were randomly divided into two parts, with 25 samples selected for each flight direction to form the training set. After down-sampling, ridge regression was used to train the readout layer. The confusion matrix of the test results is shown in Fig. 6. The classification accuracy using hysteresis MRR reached 96%, which is significantly better than the classification results obtained using linear MRR. Additionally, the UAV classification results with the hysteresis MRR are shown in Fig. 7(a), where red points represent the predicted values, and blue points represent the actual values. The Euclidean distance between the predicted and actual values is shown in Fig. 7(b). The PRC with hysteresis MRR has a smaller Euclidean distance than the standard ridge regression model with linear MRR, indicating that the memory effect of the MRR can capture subtle changes in the UAV’s flight direction, resulting in better performance.

4. Conclusion

In summary, we have theoretically and experimentally demonstrated a PRC system based on the silicon integrated MRR to perform the task of UAV flight direction recognition. Experimental results show that the proposed photonic reservoir performs well in UAV flight direction recognition, achieving an accuracy of 95.6%. The unique nonlinearity short-term memory effect observed in MRR enables the PRC to capture subtle changes in the UAV’s flight direction, highlighting its potential in hardware-based time-series processing and other photonic neuromorphic computing scenarios. The proposed photonic reservoir system operates at a MHz-level frequency, three orders of magnitude faster than traditional electronic reservoir systems^[17], and has low driving power with high energy efficiency, with power consumption at the milliwatt level. The MHz rate is limited by the finite thermal-optic time constant^[19]. Further efforts can be made to accelerate the thermo-optic (TO) response using a thinner substrate^[20] or temperature control to increase the operation speed of the PRC system. The system can be easily scaled through spatial or wavelength multiplexing for parallel processing, significantly reducing power consumption. This work emphasizes the tremendous potential of MRR in photon-based neuromorphic computing systems, providing unique nonlinearity and short-term memory, enabling high-speed, low-power, and highly complex computations. In addition, the use of high-speed, low-power, and lightweight photonic computing hardware holds the potential of UAVs to enable on-board autonomous decision-making and task execution without the need for remote control, which is of great significance for UAVs to perform complex and real-time tasks.

Acknowledgements

This work was supported by the Shanghai Municipal Science and Technology Major Project, National Key R&D Program of China (Nos. 2021YFB2802000 and 2022YFB2804300), the Shanghai Frontiers Science Center Program (2021-2025

No. 20), the Science and Technology Commission of Shanghai Municipality (No. 21DZ1100500), the National Natural Science Foundation of China (Nos. 61975123 and 62305217), the Shanghai Science and Technology Innovation Program (No. 23JC1403100), and the Shanghai Pujiang Programme. The authors acknowledge the Center for Advanced Electronic Materials and Devices for the fabrication of photonic integrated circuits.

References

1. A. Al-Kaff, D. Martin, F. Garcia, *et al.*, "Survey of computer vision algorithms and applications for unmanned aerial vehicles," *Expert Syst. Appl.* **92**, 447 (2018).
2. W. Zhang, P. Yao, B. Gao, *et al.*, "Edge learning using a fully integrated neuro-inspired memristor chip," *Science* **381**, 1205 (2023).
3. J. Garofolo and B. Wu, "Photonic analog signal processing and neuromorphic computing [Invited]," *Chin. Opt. Lett.* **22**, 032501 (2024).
4. S. Biasi, G. Donati, A. Lugnan, *et al.*, "Photonic neural networks based on integrated silicon microresonators," *Intell. Comput.* **3**, 0067 (2024).
5. X. Xu, M. Tan, B. Corcoran, *et al.*, "11 TOPS photonic convolutional accelerator for optical neural networks," *Nature* **589**, 44 (2021).
6. D. Wu, Y. Yi, and Y. Zhang, "A brief review of integrated and passive photonic reservoir computing systems and an approach for achieving extra nonlinearity in passive devices," *Sci. China Inf. Sci.* **63**, 78 (2020).
7. G. Donati, C. R. Mirasso, M. Mancinelli, *et al.*, "Microring resonators with external optical feedback for time delay reservoir computing," *Opt. Express* **30**, 522 (2022).
8. L. Zhang, Y. Fei, T. Cao, *et al.*, "Multibistability and self-pulsation in nonlinear high-Q silicon microring resonators considering thermo-optical effect," *Phys. Rev. A* **87**, 053805 (2013).
9. G. Priem, P. Dumon, W. Bogaerts, *et al.*, "Optical bistability and pulsating behaviour in Silicon-On-Insulator ring resonator structures," *Opt. Express* **13**, 9623 (2005).
10. H. K. Tsang and Y. Liu, "Nonlinear optical properties of silicon waveguides," *Semicond. Sci. Technol.* **23**, 064007 (2008).
11. M. Borghi, D. Bazzanella, M. Mancinelli, *et al.*, "On the modeling of thermal and free carrier nonlinearities in silicon-on-insulator microring resonators," *Opt. Express* **29**, 4363 (2021).
12. B. Massimo, B. Davide, M. Mattia, *et al.*, "On the modeling of thermal and free carrier nonlinearities in silicon-on-insulator microring resonators," *Opt. Express* **29**, 4363 (2021).
13. V. V. Thomas, F. Martin, M. Pauline, *et al.*, "Cascadable excitability in microrings," *Opt. Express* **20**, 20292 (2012).
14. A. Muntasa, "The human facial expression classification using the center Kernel subspace based the ridge regression," *J. Comput. Sci.* **11**, 1054 (2015).
15. R. Mussabayev, "Optimizing Euclidean distance computation," *Mathematics* **12**, 3787 (2024).
16. S. J. T. University, "Center for advanced electronic materials and devices," <https://aemd.sjtu.edu.cn/>.
17. Y. Zhong, J. Tang, X. Li, *et al.*, "A memristor-based analogue reservoir computing system for real-time and power-efficient signal processing," *Nat. Electron.* **5**, 672 (2022).
18. J. Moon, W. Ma, J. H. Shin, *et al.*, "Temporal data classification and forecasting using a memristor-based reservoir computing system," *Nat. Electron.* **2**, 480 (2019).
19. M. De Cea, A. H. Atabaki, and R. J. Ram, "Power handling of silicon microring modulators," *Opt. Express* **27**, 24274 (2019).
20. Y. S. Duh, Y. Nagasaki, Y. L. Tang, *et al.*, "Giant photothermal nonlinearity in a single silicon nanostructure," *Nat. Commun.* **11**, 4101 (2020).